Bull. Mater. Sci., Vol. 5, Nos 3 & 4, August & October 1983, pp. 185–197.

Raman spectroscopy of intermediate valent (IV) systems: Electron-phonon coupling and charge fluctuation

A JAYARAMAN
Bell Laboratories, Murray Hill, New Jersey 07974, USA

Abstract. Raman scattering measurements on intermediate valent rare earth chalcogenides crystallizing in the NaCl structure are reviewed. The experimentally obtained Raman intensities are compared with the theoretically calculated intensities, using a lattice dynamical model in which the electron lattice interaction has been expressed in terms of local intraionic charge deformabilities, with monopolar (breathing Γ_1^+), dipolar (Γ_{15}^-), and quadrupolar (Γ_{12}^+) symmetry. Phonon anomalies in SmS, $Sm_{0.75}Y_{0.25}S$ and YS are described and discussed. Finally, evidence for a new excitation involving 4f charge fluctuations is presented, which is observed as a dispersionless excitation in the acoustic-optic phonon gap in (IV) materials.

Keywords. Raman scattering; intermediate valent materials; charge fluctuation; electron-phonon coupling

1. Introduction

Many rare earth systems exhibit intermediate valent (IV) behaviour at ambient or high pressure (Birgeneau and Shapiro 1977; Stüsser *et al* 1982). In these systems the valence state of the rare earth ion fluctuates rapidly due to the exchange of an electron between the $4f^n$ and $4f^{n-1}$ configurations of the rare earth ion (Güntherodt *et al* 1981b). This charge fluctuation could be on the same time scale as lattice vibrations and hence can couple to the latter (Stüsser *et al* 1982). Also, since a valence change involves a large change in the volume of the fluctuating rare earth ion, a strong electron-phonon interaction may be expected in (IV) materials, giving rise to phonon anomalies (Kress *et al* 1981). These effects have been seen in recent Raman studies, in substituted SmS (Güntherodt *et al* 1981c), TmSe (Stüsser *et al* 1981) and more recently in $CeBe_{13}$ (Jayaraman *et al* 1983). A lattice dynamical model involving local deformabilities of the ionic charge density successfully accounts for the observed results (Bilz *et al* 1979). A new excitation has been seen in the spectral gap between the acoustic and optical phonons and this is believed to be due to a polaronic charge fluctuation (Stüsser *et al* 1982). These results will be reviewed in this paper.

2. Raman scattering in substituted SmS and TmSe

The substituted SmS and TmSe crystallize in the NaCl structure, in which the first-order Raman scattering ($q = 0$) is symmetry forbidden. However the presence of defects or impurities in the lattice destroys the inversion symmetry locally and consequently removes this restriction. The intensity of the first-order defect induced Raman scattering in the NaCl structure is given by a one-phonon density of states weighted by the electron-phonon matrix element. In the lattice dynamical model of Bilz *et al* (1979) this has been expressed in terms of local deformabilities associated with the ionic charge density.

3. Electron lattice coupling

The electron-lattice interaction in $Sm_{1-x}Y_xS$ in its semiconducting ($x = 0$), mixed valent ($x = 0{\cdot}25$) and superconducting ($x = 1$) phases has been described in terms of the local deformabilities of the ionic charge density (see Güntherodt *et al* 1981b and the references cited therein). Assuming only radial couplings between nearest neighbours in the NaCl lattice, the short range electron-lattice interaction can be represented in adiabatic approximation and point multipole expansion, in terms of three local interionic deformabilities of monopolar or breathing (Γ_1^+), dipolar (Γ_{15}^-) and quadrupolar (Γ_{12}^+) symmetry which are shown in figure 1. In this concept the response of the electrons is represented by symmetry coordinates of local lattice deformations, which contribute to the self-energy part of the dynamical matrix. The advantage of the method is that at points of high symmetry in the Brillouin zone the deformabilities can be unambiguously attributed to specific phonon branches, as indicated in table 1. The microscopic origin and existence of these deformabilities depends on whether the electronic band structure near E_F allows for virtual excitations, with changes in the angular momentum l of monopolar (Γ_1^+, $\Delta l = 0$), dipolar (Γ_{15}^-, $\Delta l = \pm 1$) or quadrupolar (Γ_{12}^+, $\Delta l = \pm 2$) character. The phonon-induced virtual excitations (dynamic hybridization) with $\Delta l = 0$, ± 1 or ± 2, giving rise to periodic charge redistributions superimposed on the charge relaxations, will appear in the phonon anomalies.

4. Phonon anomalies and the lattice dynamical model

On the basis of a shell model, which uses two nearest neighbour force constants and the

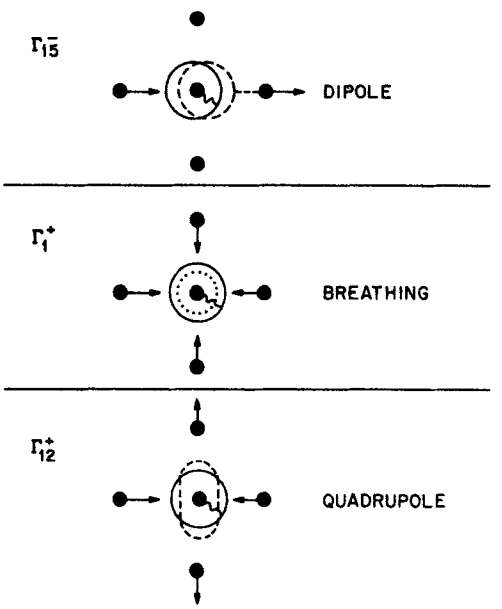

Figure 1. Local symmetries of the displacement-induced intraionic charge deformabilities in NaCl-type lattice (Bliz 1972).

Table 1. Local deformabilities in NaCl lattice.

Symm. of deform.	Effect on	Observed in SmS | $Sm_{0.75}Y_{0.25}S$ | YS			Microscopic origin
Γ_1^+ (Sm)	LO(L) LA($\xi\xi\xi$)	x	x		$4f^6 \rightarrow 4f^5\,(5d^1)$
Γ_{15}^- (Sm)	LO(Γ)	x	x		$4f^6 \rightarrow 5d^1\,(4f^5)$
Γ_{12}^+ (Sm)	TO(L)				
Γ_1^+ (S)	LA(L)			x	$3d_{xy} \rightarrow 3d_{xy}$
Γ_{15}^- (S)	LO (Γ)				
Γ_{12}^+ (S)	TA(L)				

three deformabilities mentioned above, the phonon dispersion curves of semiconducting SmS and mixed valent $Sm_{0.75}Y_{0.25}S$, together with their reference materials EuS and YS respectively have been calculated, and the curves are shown in figure 2b. For the [111] direction, best fits to the existing neutron data for SmS (Birgenau and Shapiro 1977), $Sm_{0.75}Y_{0.25}S$ (Mook *et al* 1978a) and YS (Roedhammer *et al* 1978) are obtained. The phonon anomalies are identified in the latter three compounds in terms of the local charge deformabilities, whose microscopic origin is discussed below on the basis of the electronic band structure shown schematically in figure 2a.

The TA, LA and TO branches of EuS and SmS have similar dispersions (Bilz *et al* 1979). However the entire LO branch of SmS shows a softening with respect to that of EuS (see dashed curve). This is attributed to the combined action of a Sm dipolar and breathing deformability at the Γ and the L point, respectively. The enhanced polarizability of the Sm ion stems from the small (0·1 eV) *f-d* promotion gap in SmS, compared to 1·7 eV for EuS.

On the other hand metallic YS represents a simple reference material for $Sm_{0.75}Y_{0.25}S$, because of its degenerate optic and acoustic phonon branches. This behaviour can be described in a first approximation by a nearest-neighbor force constant model, except for the LA phonon anomaly near the L point. The LA(L) anomaly is associated with the electron-phonon interaction in this superconductor, and is attributed to a sulphur breathing deformability due to $S(3d_{xy})^- S(3d_{xy})$ excitations near E_F. The softening in $Sm_{0.75}Y_{0.25}S$ (starting from the degenerate optic branch of YS [dashed curve]) near the Γ point is due to a Sm dipolar deformability and this accounts for the positive slope of the TO branch. The softening of the LO branch as it approaches the L point is a consequence of Sm breathing deformability. The latter is also responsible for the softening of the LA branch below the TA branch for $k < 3/5\,k_L$. The normal behaviour of the LA branch shown by dotted lines is seen in SmS, and in the case of YS except near the L point.

In figure 3 is shown the 5 parameter-fit of the phonon dispersion curves of $Sm_{0.75}Y_{0.25}S$ to the experimental neutron data of Mook *et al* (1978a). The [111] direction (exhibiting the most pronounced phonon anomalies) is rather crucial for the quality of the fit. The agreement between theory and experiment is fairly good, in particular for the TO, LO and the TA branches along the [111] direction. The fit reproduces qualitatively the anomalous behavior of the LA branch in the [111] direction.

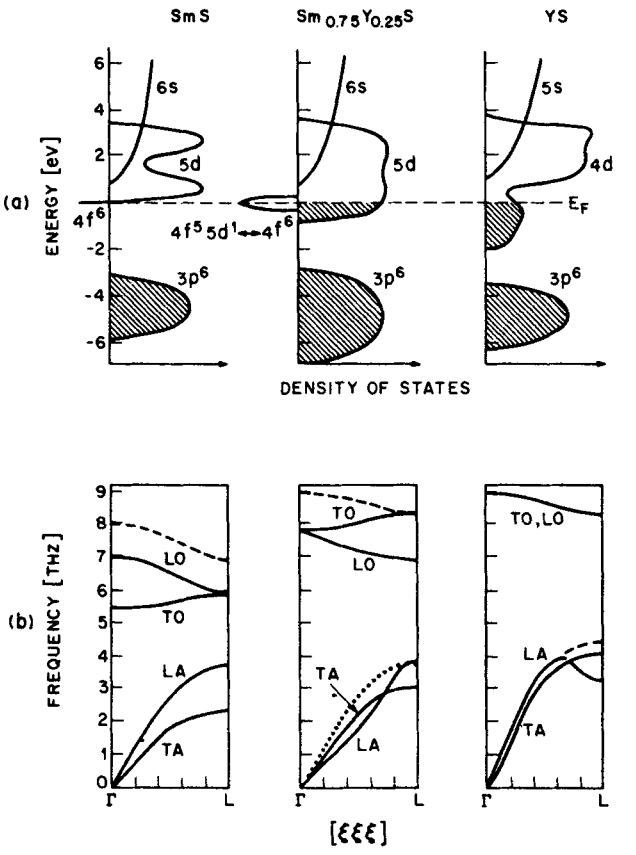

Figure 2. Schematic electronic densities of states and calculated phonon dispersion curves of SmS, $Sm_{0.75}Y_{0.25}S$ and YS. Reference materials exhibiting normal dispersion are indicated by dashed or dotted lines. From Bilz *et al* (1979).

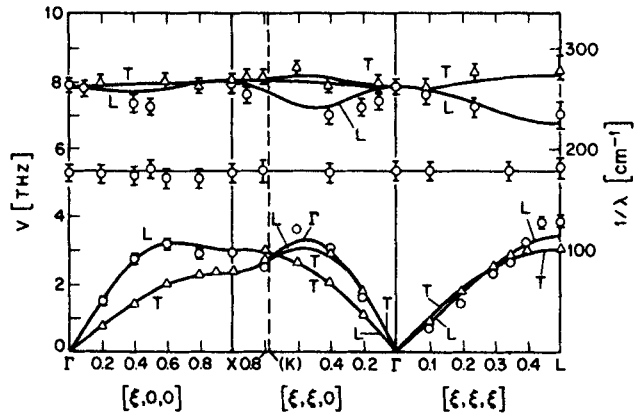

Figure 3. Calculated phonon dispersion curves of $Sm_{0.75}Y_{0.25}S$ using a 5-parameter model; experimental points from Mook *et al* (1978a).

5. Raman measurements

The essential role of Raman scattering in the present context is that it tests not only the phonon frequencies and symmetries of phonon eigenvectors, but most of all the symmetry and strength of the electron-phonon matrix element. The intensity of first order Raman scattering is in general determined by the phonon-modulated electric susceptibility $I \sim |\partial\chi_u/\partial u|^2$, where u is the displacement of the atoms from their equilibrium position. χ describes the response of the electronic system. This implies that the Raman scattering intensity tests microscopically, the symmetry and coupling strength of the phenomenological deformability concept introduced in § 3. We expect strong scattering intensity from those deformabilities which also describe the phonon anomalies.

5.1 $Sm_{1-x}Y_xS$

The Raman intensities of $Sm_{1-x}Y_xS$ have been calculated for $x = 0$, 0·25 and 1, by projecting those eigenvectors from the one-phonon density of states, which are compatible with the symmetry of the specific intraionic charge deformability under consideration. The one-phonon densities of states of the calculated dispersion curves in figure 2 are shown for SmS, $Sm_{0.75}Y_{0.25}S$ and YS by the histograms of figures 4, 5 and 6, respectively. The calculated Raman intensities, *i.e.* the "projected" one-phonon densities of states with breathing (Γ_1^+) and quadrupolar (Γ_{12}^+) symmetry are shown by the shaded area and dashed line, respectively, in the lower part of figures 4, 5 and 6. The polarized Raman spectra in the upper part have been separated into the different symmetry components of the scattering tensor (Güntherodt *et al* 1981c). The Γ_{25}^+ symmetry describes next-nearest neighbour interactions. The dipolar (Γ_{15}^-) symmetry is only infrared-active, but can contribute to second order scattering (see also § 2).

The dominant scattering intensity with Γ_1^+ symmetry of SmS near 200 cm^{-1} in figure 4 (thick line) arises from the breathing deformability of the Sm ion, as seen by the good

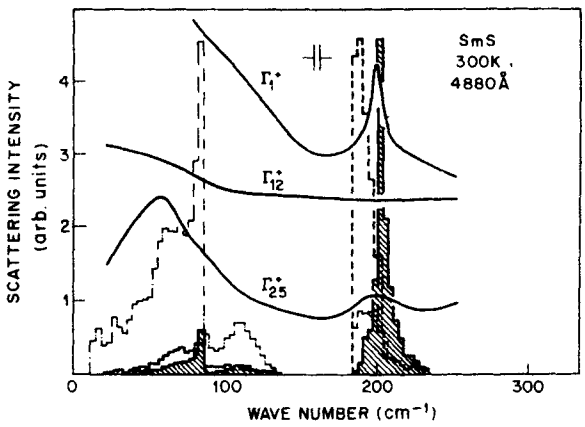

Figure 4. Polarized Raman spectra of SmS. Experiment: solid lines; theory: histograms (dashed-dotted line: one-phonon density weighted by $(n(\vec{q}j)+1)/\omega(\vec{q}j)$; full line (shaded area): Γ_{12}^+-contribution; dashed line: Γ_{12}^+-contribution). From Güntherodt *et al* (1981c) (Γ_1^+ (Sm), Γ_{12}^+ (Sm)).

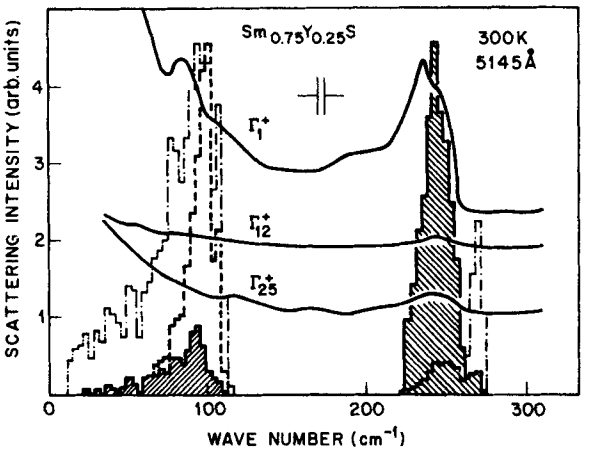

Figure 5. Polarized Raman spectra of $Sm_{0.75}Y_{0.25}S$. Notation as in figure 4 (Güntherodt *et al* 1981c) (Γ_1^+ (Sm), Γ_{12}^+ (S)).

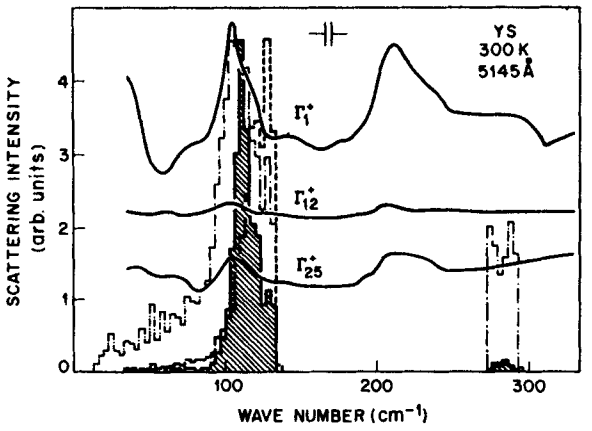

Figure 6. Polarized Raman spectra of YS. Notation as in figure 4. Intensity near 200 cm^{-1} is due to second order scattering (Güntherodt *et al* 1981) (Γ_1^+ (S), Γ_{12}^+ (S)).

agreement with the calculation (shaded area). The assumption that a (Γ_{12}^+) quadrupolar deformability of the Sm ion gives rise to a peak near 190 cm^{-1} (dashed line) does not agree with the experimental observation. In $Sm_{0.75}Y_{0.25}S$ the strong Γ_1^+ scattering intensity from optic phonons and the weaker one from acoustic phonons is due to a Sm breathing deformability, in good agreement with the calculation (shaded area). The peak near 100 cm^{-1} (thin line) presumably due to the sulphur quadrupolar deformability is not reproduced in the experimental Γ_{12}^+ spectrum. The missing contributions to the experimental Γ_{25}^+ spectrum in figure 5 indicates that the neglect of intersite Sm-Sm or S-S interactions in the model for $Sm_{0.75}Y_{0.25}S$ is justified.

The most prominent Γ_1^+ scattering intensity of YS near 100 cm^{-1} in figure 6 is well described by the calculation (shaded area) under the assumption of a breathing

deformability of the S ion, which also gives rise to the LA(L) phonon anomaly (§ 4). Slight differences in the experimental and calculated peak positions near 100 cm^{-1} may be due to different stoichiometries in the bulk as seen by neutron scattering [Roedhammer *et al* 1978] and near the surface of the very same crystal as measured in Raman scattering. Our calculations are based on fits to the neutron data of Roedhammer *et al* (1978). The weak experimental Γ_1^+ intensity near 280 cm^{-1} agrees well with the calculated weak intensity from the optic phonons. The calculated intensity under the assumption of a quadrupolar deformability of the S ion gives rise to a peak near 130 cm^{-1}. The lack of intensity in the experimental Γ_{12}^+ spectrum indicates the nonexistence of the corresponding microscopic excitations.

5.2 *TmSe*

Raman scattering measurements on freshly cleaved single crystals of Tm_xSe have been performed (Stüsser *et al* 1981). Polarized Raman spectra of $Tm_{1\cdot0}Se_{1\cdot0}$ are shown in figure 7 for the three different symmetries of the scattering tensor. The peak near 175 cm^{-1} has been identified by its softening with increasing valence mixing, which parallels that of the bulk modulus, as originating mainly from zone boundary LO phonons (Treindl and Wachter 1979). This is consistent with its dominant Γ_1^+ scattering intensity as seen in figure 7 and with the findings in $Sm_{0\cdot75}Y_{0\cdot25}S$ (figure 5). From the latter we conclude that the strong Γ_1^+ intensity near 175 cm^{-1} and 70 cm^{-1} in figure 7 is due to the Tm(Γ_1^+) breathing deformability associated with $4f^{13} \rightarrow 4f^{12}5d^1$ excitations near E_F. Depending on the mechanical polishing conditions of the TmSe

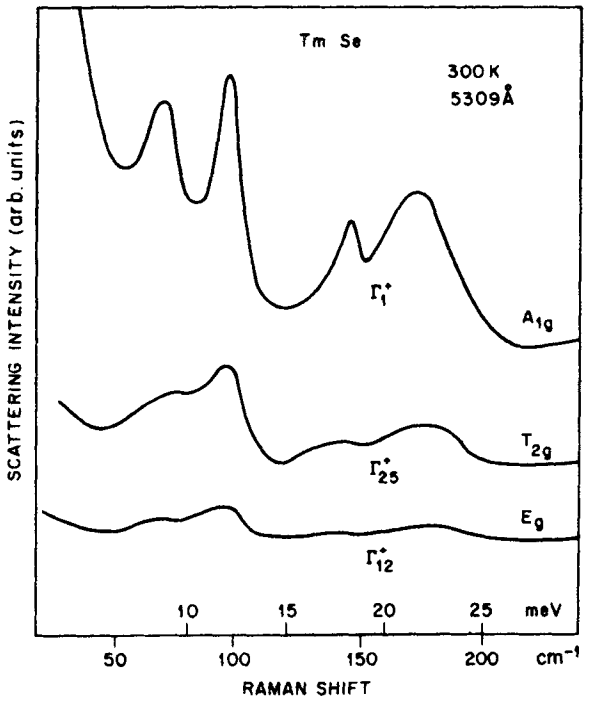

Figure 7. Symmetry analyzed Raman scattered intensity in TmSe, from polarized spectra. (Stusser *et al* 1981)

single crystals, the 70 cm^{-1} peak can be shifted almost continuously to 60 cm^{-1}. This behaviour is attributed to a further softening of the LA($\xi\xi\xi$) branch for $k < 4/5k_L$ (Triendl and Wachter 1980). This is consistent with our Γ_1^+ scattering intensity from acoustic phonons near 70 cm^{-1} in Tm_1Se_1 (figure 7) due to a Tm(Γ_1^+) breathing deformability, in analogy to the behaviour of $Sm_{0.75}Y_{0.25}S$ below 100 cm^{-1} in figure 5. The Γ_1^+ and Γ_{25}^+ contributions to the peak near 100 cm^{-1} (McWhan *et al* 1978) in figure 7 are attributed to a Se breathing deformability and to nearest-neighbour Se-Se interactions. The peak near 145 cm^{-1} has been attributed to TO phonons, and in a later study (Treindl and Wachter 1979) to twice the LA phonon. A rather general and novel interpretation of this peak near 145 cm^{-1} is discussed in the next section.

6. Polaronic charge fluctuation excitation

So far we have been concerned with the investigation of phonon anomalies. Charge relaxations of the valence fluctuating ions are expected to show up in quasielastic light scattering (Lopez and Balseiro 1978). However a coupling of these charge density fluctuations to phonons can shift spectral weight from quasielastic to inelastic scattering, on the phonon frequency scale. This has been reported by Stüsser *et al* (1982) and will form the subject matter of this section.

Neutron scattering experiments (Mook *et al* 1978a) in (IV) $Sm_{0.75}Y_{0.25}S$ at room temperature have shown a dispersionless mode near 175 cm^{-1} (21.9 MeV) within the gap of optic and acoustic phonon branches, but this mode has been assigned to a local mode of the Y ion, by mass scaling with the heavier Sm ion. The Raman spectrum of $Sm_{0.75}Y_{0.25}S$ (Güntherodt *et al* 1981c) shows a shoulder near 185 cm^{-1} (see figure 5) which agrees within experimental errors with the dispersionless mode observed in neutron scattering experiments. The same shoulder is observed in the Raman spectrum of $Sm_{0.65}Y_{0.35}S$ in figure 8 near 200 cm^{-1}. Further the (IV) phases of $Sm_{1-x}R_xS$ with 25 atomic % Pr, 10 at. % Pr + 10 at. % Gd and 24 at. % Dy in figure 8 show similar features and in particular the "gap mode" frequency is nearly the same for all of them. The absence of a significant cation mass scaling for the above mode in $Sm_{1-x}R_xS$, with R = Pr, Gd and Dy rules out the possibility that it is a local mode of the substituted cations (in the frequency range of the "gap mode"). The practically unchanged scattering intensity of the "gap mode" of $Sm_{0.78}Gd_{0.22}S$ upon cooling from 300 K to 80 K shown in figure 8 proves its first-order nature, and this is true for all the (IV) phases of $Sm_{1-x}R_xS$ with $x < 0.5$. The symmetry analysis of the "gap mode" scattering intensity in all the $Sm_{1-x}R_xS$ systems shows that the A_{1g} symmetry component is the dominant contribution to the Raman intensity. This is shown for $Sm_{0.78}Gd_{0.22}S$ in the lower part of figure 8.

In $SmS_{1-y}As_y$, the above mentioned "gap mode" is observed over the entire (IV) range ($0.1 \leqslant y < 1$) as shown in figure 9 for $y = 0.1$, 0.2 and 0.6. It appears between the acoustic (below 150 cm^{-1}) and optic (above 220 cm^{-1}) phonon density of states. In $Sm^{3+}As$ only the optic phonon density of states near 230 cm^{-1} is observed. Again the "gap mode" could be identified as a first-order process of A_{1g} symmetry, with a frequency position following the LO(L) phonon frequency. Further the spectra in figure 9 prove that the "gap made" near 200 cm^{-1} is not related to a local mode, for a mode due to As should appear near 165 cm^{-1} and should broaden with increasing As concentration (see figure 9). The persistence of the "gap mode" of practically unchanged

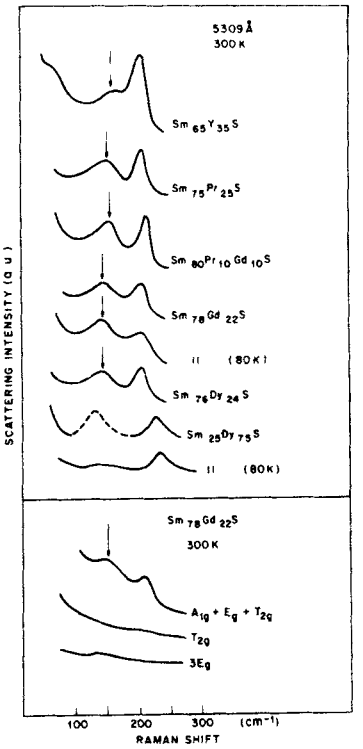

Figure 8. Raman spectra of cleaved (100) faces of (IV) $Sm_{1-x}R_xS$ (R = Y, Pr, Gd, Dy) at 300 K. Top: Unpolarized spectra; spectra at 80 K for $x = 0{\cdot}22$ Gd and $x = 0{\cdot}75$ Dy, respectively, prove first- and second-order scattering. Bottom: Symmetry-analyzed spectra of $Sm_{0{\cdot}78}Gd_{0{\cdot}22}S$. The "gap mode" is marked by arrows.

width for all concentrations for As ($0{\cdot}1 \leqslant y < 0$) in the $Sm_{1-x}As_y$ shows, that its disappearance in $Sm_{1-x}R_xS$ system for $x > 0{\cdot}5$ is not due to an alloying effect. On the contrary, its disappearance in the latter system is due to a reduction of Sm-Sm interactions. It is to be noted that the Sm concentration remains unchanged at 100% throughout the (IV) phase of $SmS_{1-y}As_y$.

The above results have shed new light on the inelastic excitation near 145 cm^{-1} in the Raman spectrum of TmSe. In figure 10 the Raman spectrum of TmSe for different valence fraction of the Tm ion as obtained through anion substitution by S or Te is shown. The 145 cm^{-1} excitation in $Tm_{1{\cdot}01}Se$, from its temperature dependence appears to be a first-order process and has the A_{1g} symmetry character. This excitation shifts in parallel with the LO(L) phonon frequency, as shown for $TmSe_{0{\cdot}5}S_{0{\cdot}5}$ and $TmSe_{0{\cdot}85}Te_{0{\cdot}15}$ in figure 10. It is observed at 145 cm^{-1} in all (IV) phases of $TmSe_{1-y}Te_y$ and $TmSe_{1-y}S_y$, *i.e.*, without any dilution of the Tm concentration, and disappears in $Tm^{3+}S$. These feaures characterize the 145 cm^{-1} excitation of TmSe as a "gap mode", in analogy to the $Sm_{1-y}R_xS$. The previous assignment to it as a two-phonon (Treindl and Wachter 1979) process, due to strong anharmonicity effects appears to be unlikely, since no two-phonon scattering from the anomalous LO(L) phonons has been observed. Calculations of the symmetry-projected Raman intensities of TmSe, on the basis of a lattice-dynamical model-fit to the measured phonon

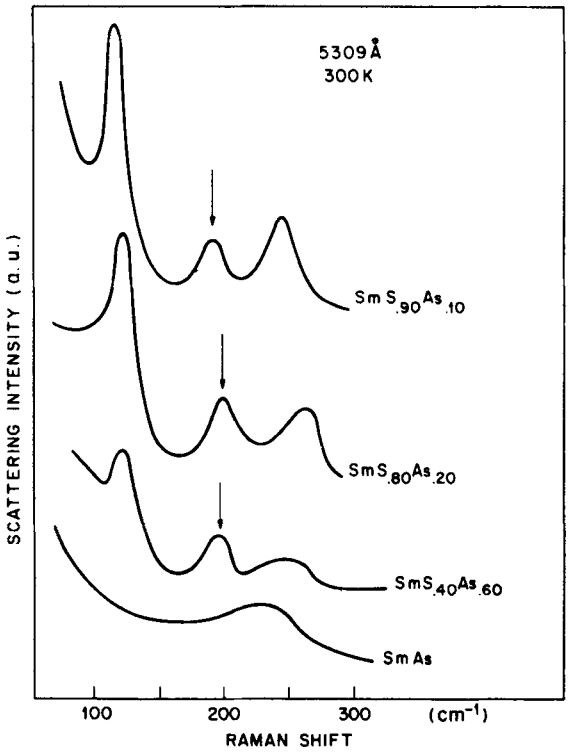

Figure 9. Unpolarized Raman spectra of cleaved single crystals of $SmS_{1-x}As_x$ (x = 0·1, 0·2, 0·6, 1) at 300 K. The "gap mode" is marked by arrows.

dispersion (Mook and Holtzberg 1981) have shown, that the 145 cm^{-1} excitation can only be reproduced as a (bound) phonon state split off from the bulk LO phonon branches, due to higher-order nonlinear lattice dynamics.

Further, the following possibilities for the origin of the "gap mode" are ruled out: (i) The parallel shift in frequency of the optic, LO(L), phonon and the "gap mode" may suggest a coupled plasmon-LO phonon mode. However, the involvement of the so-called "acoustic plasmon" (Varma 1976), with a frequency comparable to that of the optic phonons implies for small wave vectors, an electron concentration dependence $\omega_q^{ac} \sim n^{-1/3}$, where n is the conduction electron concentration. But the "gap mode" frequency is found to be independent of the concentration of the substituted R^{3+} ions; the latter contributes one conducting electron per R^{3+} and this should shift the frequency. Further, the "gap mode" of TmSe is also not affected by cooling to 1·5 K, despite the strong increase in resistivity below the Neel temperature $T_N = 3{\cdot}5$ K (Holtzberg *et al* 1979). (ii) In the case of the (IV) phase of $Sm_{1-x}R_xS$, electronic Raman scattering from the $J = 1$ level of the (Sm^{2+}) $4f^6$ configuration, which possibly could overlap with the "gap mode" is excluded by polarized Raman scattering measurements (Güntherodt *et al* 1981a). Further, in the case of TmSe no electronic levels are expected near the "gap mode" frequency.

Thus the "gap mode" appears to be an intrinsic feature associated with valence fluctuations, in all the NaCl-structure type rare earth chalcogenides so far studied. Its

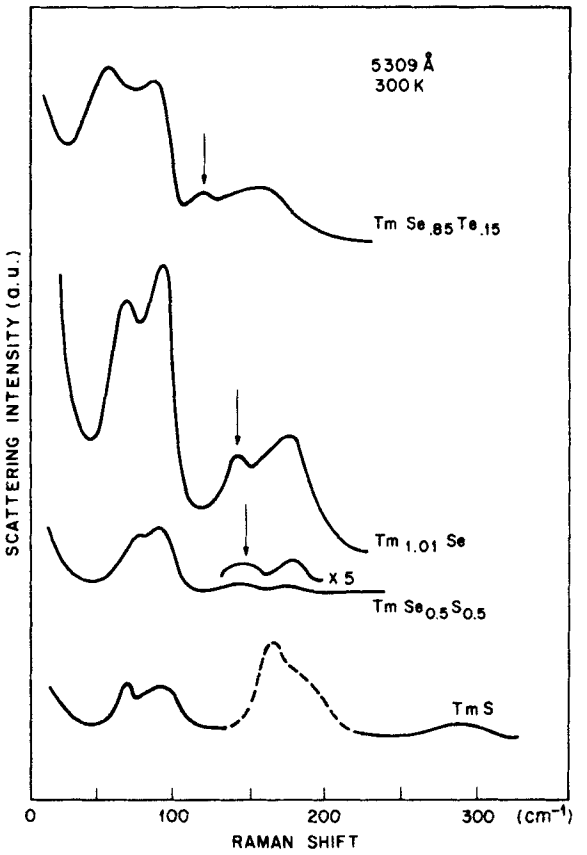

Figure 10. Unpolarized Raman spectra of cleaved single crystals of $TmSe_{1-x}S_x$ ($x = 1, 0.5$), $Tm_{1.01}Se$ and $TmSe_{0.85}Te_{0.15}$ at 300 K. Dashed line for TmS indicates second order scattering. The "gap mode" is marked by arrows.

appearance in the A_{1g} symmetry component is consistent with scattering by electron density fluctuations (Platzman 1965; McWorther 1966). For the genesis of the "gap mode" the following mechanism has been suggested (Stüsser *et al* 1982), namely that it arises due to a coupling of the incoherently fluctuating localized 4*f*-charge density of the (IV) rare earth ions to the LO(L) phonon breathing mode, through ionic size effects. (The charge fluctuation is a consequence of electron-hole pair excitations of the $4f^n \rightleftarrows 4f^{n-1}5d^1$ type and this gives rise to an ionic size change. Since the LO(L) breathing mode is dominated by lattice distortions and size effects, it couples to the charge fluctuation, *via* the size effect.) The coupling of this localized excitation to the LO(L) phonon in real space gives rise to a dispersionless excitation in k-space, which may be described as a 'polaronic bound excitation', or "bound fluctuon". This is consistent with the dispersionless mode observed in neutron scattering of $Sm_{0.75}Y_{0.25}S$ (Mook *et al* 1978a). Magnetic scattering in $Sm_{0.75}Y_{0.25}S$ has been observed by neutron scattering near 31 MeV (250 cm^{-1}) in powder samples (Mook *et al* 1978b) and near 25 MeV (200 cm^{-1}) in single crystals. The latter result is consistent with a 4*f* form factor of the localized charge density of the "bound fluctuon", identified in $Sm_{0.75}Y_{0.25}S$ single crystals.

7. Summary and conclusions

The description of phonon anomalies and Raman intensities in terms of the concept of local cluster deformabilities is applicable equally to incipient valence-instabilities of Sm ions in semiconducting SmS, to mixed-valent Sm and Tm ions in $Sm_{0.75}Y_{0.25}S$ and TmSe, respectively, and to polarizable S and Se anions of the above compounds. Differences in the specific phonon anomalies and Raman spectra have been shown to arise from differences in the position in energy, in symmetry and in the degree of localization of the electronic states involved in the electron-phonon coupling. The analysis for mixed valent $Sm_{0.75}Y_{0.25}S$ supports the essential role of a rather localized electron-phonon coupling and of a dominant phonon-induced on-site *f-d* hybridization. Apart from the evidence for a (Γ_{15}^{-}) dipolar deformability of the mixed-valent Sm ion, the dominance of a deformability or charge fluctuation with (Γ_1^+) monopolar symmetry, contributing most strongly to the Raman intensities, is consistent with conclusions drawn from the phenomenological charge fluctuation model of lattice dynamics (Wakabayashi 1980) and from a microscopic calculation of the charge relaxation rates (Muller-Hartmann 1981).

The new mode, "gap mode" appearing between the acoustic and optic phonon gap of NaCl structure type (IV) compounds is due to first-order scattering of A_{1g} symmetry and is attributed to a coupling of the incoherently fluctuating localized $4f$ charge density to local lattice distortions and hence is given the suggestive designation "polaronic bound exciton", or "bound fluctuon".

Acknowledgements

It is a pleasure to acknowledge illuminating discussion with Dr G Güntherodt who is the principal architect in the field of study discussed in this article and with whom the present author has extensively collaborated. I am very much indebted to Prof. H Bilz and Dr W Kress for several discussions on the subject. I wish to thank R G Maines for much assistance in the preparation of the figures for this paper.

References

Bilz H 1972 *Computational solid state physics* (eds) F Herman, N W Dalton and T R Koehler (New York: Plenum Press) p. 309

Bilz H, Güntherodt G, Kleppmann W and Kress W 1979 *Phys. Rev. Lett.* **43** 1998

Birgeneau R J and Shapiro S M 1977 *Valence instabilities and related narrow band phenomena* (ed.) R Parks (New York: Plenum Press) p. 49

Falicov L M, Hanke W and Maple M B (eds) 1981 *Valence fluctuations in solids* (North Holland: Amsterdam)

Güntherodt G, Jayaraman A, Anastassakis E, Bucher E and Bach H 1981a *Phys. Rev. Lett.* **46** 855

Güntherodt G, Jayaraman A, Bilz H and Kress W 1981b *Valence fluctuations in solids* (eds) L M Falicov, W Hanke and M B Maple (North Holland: Amsterdam) p. 121

Güntherodt G, Jayaraman A, Kress W and Bilz H 1981c *Phys. Lett.* **A82** 26

Holtzberg F, Penney T and Tournier R 1979 *J. Physique* 40 coll. **C5** 314

Jayaraman A, Güntherodt G, Batlogg B and Croft M 1983 *Bull. Am. Phys. Soc.* **28** 283

Kress W, Bilz H, Güntherodt G and Jayaraman A 1981 *J. Physique* **C6** supplement au no 12 V42 C6-3-10

Lopez A and Balseiro C 1978 *Phys. Rev.* **B17** 99

McWhan D B, Shapiro S M, Eckert J, Mook H A and Birgeneau R J 1978 *Phys. Rev.* **B18** 3623

McWorther A L 1966 *Physics of quantum electronics* (eds) P L Kelly, B Lax and P E Tannenwald (New York: McGraw Hill) p. 111

Mook H A and Holtzberg F 1981 in *Valence fluctuations in solids* (eds) L M Falicov, W Hanke and M B Maple (Amsterdam: North Holland) p. 113
Mook H A, Nicklow R M, Penney T, Holtzberg F and Shafer M W 1978a *Phys. Rev.* **B18** 2925
Mook H A, Penney T, Holtzberg F and Shafer M W 1978b *J. Phys. (Paris)* Coll. Suppl. 8, 30 **C6** 837
Muller-Hartmann E 1981 in *Proc. of the Taniguchi Symp.* (ed) T Moriya, Springer Verlag series in *solid state science*, Vol **29** 178
Parks R D 1977 (ed) *Valence instabilities and related narrow band phenomena* (New York and London: Plenum Press)
Platzman P M 1965 *Phys. Rev.* **A139** 379
Roedhammer P, Reichardt W and Holtzberg F 1978 *Phys. Rev. Lett.* **40** 465
Stüsser N, Barth M, Güntherodt G and Jayaraman A 1981 *Solid State Commun.* **V39** 965
Stüsser N, Güntherodt G, Jayaraman A, Fisher K and Holtzberg F 1982 in *Valance instabilities* (eds) P Wachter and H Boppart (Amsterdam: North Holland) p. 69.
Treindl A and Wachter P 1979 *Solid State Commun.* **32** 573
Treindl A and Wachter P 1980 *Solid State Commun.* **36** 901
Varma C M 1967 *Rev. Mod. Phys.* **48** 219
Wachter P and Boppart H 1982 (eds) *Valence instabilities* (Amsterdam: North Holland)
Wakabayashi N 1980 *Phys. Rev.* **B22** 5833